LAWRENCE
LIVERMORE
NATIONAL
LABORATORY

UCRL-TR-227308

Simulated Performance of a Second-Generation Compact Compton Imaging Detector

H. A. Manini

January 18, 2007

This work was performed under the auspices of the U.S. Department of Energy by University of California, Lawrence Livermore National Laboratory under Contract W-7405-Eng-48.

h4doc doc12v1
UCRL-TR-227308

Simulated Performance of a Second-Generation Compact Compton Imaging Detector

Hugh Manini

N Division
Lawrence Livermore National Laboratory

January 8, 2007

Abstract

Simulations are performed using GEANT4 of a second-generation compact Compton imaging detector called CCI2 which uses silicon and germanium detector crystals. Realistic simulated detector geometry and realistic detector parameters are used. Results are obtained for the CCI2 detector for the intrinsic photopeak efficiency, imaging efficiency, and angular resolution, and simulated images are created for point sources with various energies and source angles.

1 Detector simulations

I perform full physics simulations using GEANT4 of the CCI2 detector. Source photons from a point source are generated at a specific energy and tracked through the detector volumes. The positions and energies for each interaction are stored for further analysis. The exact information is then "digitized", and detector resolution effects are introduced, so that the resulting simulated output mimics the realistic detector response. The exact x and y coordinates of the interactions within the active detector crystals are pixelized. The silicon detector crystals and the germanium detector crystals each have detection strips that are 2 mm wide. This produces pixels in the xy-plane that are 2 mm$\times$2 mm in size (the xy-plane is parallel to the front surface of each detector crystal). When more than one interaction occurs within a pixel, the interactions and deposited energies are combined. The interaction depth within the detector is represented by the z coordinate, and the exact z coordinate of each interaction is smeared using a Gaussian probability distribution with a FWHM of 0.5 mm. The detected energy distribution is determined by smearing individual energy deposits using a Gaussian probability distribution with a specified FWHM at each energy, to model the energy resolution. For both the silicon detector crystals and the germanium detector crystals, the FWHM energy resolution is 2 keV, for all energies.

1.1 Simulated detector geometry

The simulated detector geometry for the CCI2 detector is shown as a cross-sectional side view in Figure 1, and as a cross-sectional front view in Figure 2. The simulated detector geometry for the CCI2 detector includes two aluminum cryostats, two silicon detector crystals, two germanium detector crystals, an aluminum mount for the silicon detector crystals, an aluminum mount for the germanium detector crystals, two solid copper tubes, and a circular aluminum base plate.

Each silicon detector crystal is rectangular in shape and is 76 mm$\times$76 mm$\times$10 mm in size. The active portion of each silicon detector crystal is 64 mm$\times$64 mm$\times$10 mm in size. The silicon detector crystals are very useful for providing imaging capability for photon energies below 150 keV. Each germanium detector crystal is cylindrical in shape and 15 mm thick, with the front 10 mm of thickness having an outer radius of 45 mm, and the remaining 5 mm of thickness having an outer radius of 50 mm. For each germanium detector crystal, the active portion is the portion of volume within a 42 mm radius which is inside a concentrically inscribed box that is 76 mm$\times$76 mm$\times$15 mm in size. This gives an active area for each germanium detector crystal of 51.56 cm^2. The separation distance is 28.6 mm between the front wall of the front cryostat and the front silicon detector crystal. The separation distance between the two silicon detector crystals is 8.4 mm. The separation distance is 28.1 mm between the second silicon detector crystal and the first germanium detector crystal. The separation distance between the two germanium detector crystals is 10.5 mm.

There are two aluminum cryostats that are separated from each other by a 1 mm gap. The front cryostat contains the two silicon detector crystals and the aluminum mount for the silicon detector crystals, and the other cryostat contains the two germanium detector crystals and the aluminum mount for the germanium detector crystals. Each cryostat is 22.7 cm tall in the y direction, 20.3 cm long in the x direction, and 7.3 cm wide in the z direction. Each cryostat has top and bottom walls that are 13 mm thick, side walls that are 7 mm thick, and front and back walls that are each 5 mm thick everywhere except within a circular region in which the wall thickness is 1 mm. Each of these circular regions is 71.5 mm in radius and centered on the detector crystals. The front and back cryostat walls are thinner within these circular regions to allow more photons to reach the detector crystals. All of the detector crystals are aligned so that the center point of each detector crystal is along the z axis. The separation distance is 18.5 mm in the x direction between the z axis and the center point of the front cryostat, and the separation distance is 4.5 mm in the y direction between the z axis and the center point of the front cryostat. The silicon detector crystals have a rectangular aluminum mount that is 5 mm thick and separated from the side edges of the silicon detector crystals by 5 mm. The germanium detector crystals have a cylindrical aluminum mount that is 2 mm thick and separated from the side edges of the germanium detector crystals by 5 mm.

The two solid copper tubes are part of the cooling system. Each copper tube is 32 mm in diameter and 12 cm long. Each copper tube extends 18 mm into the inside of a cryostat. Below the cryostats is a circular aluminum base plate which has a diameter of 17.5 cm and is 6 mm thick.

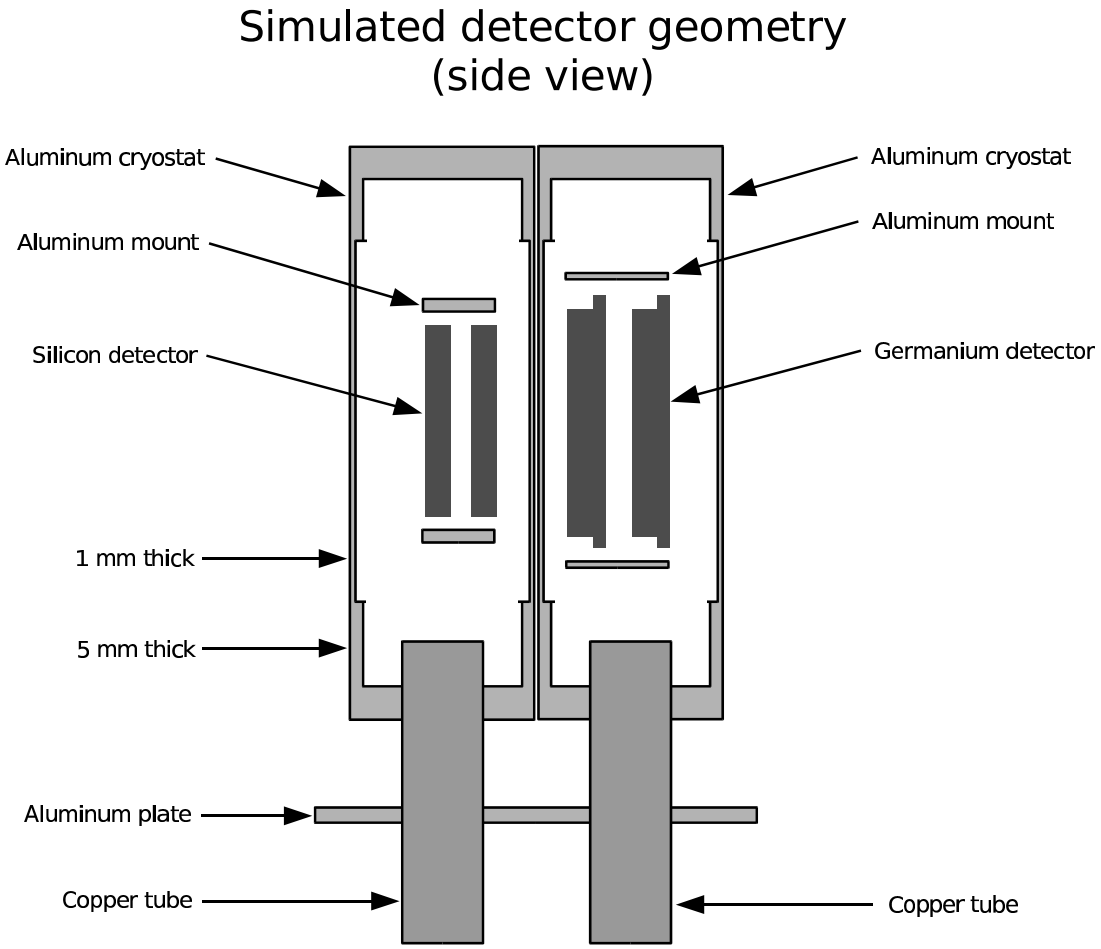

Figure 1: Simulated detector geometry for the CCI2 detector, shown as a cross-sectional side view. The cross-section passes through the center point of each silicon detector crystal and each germanium detector crystal.

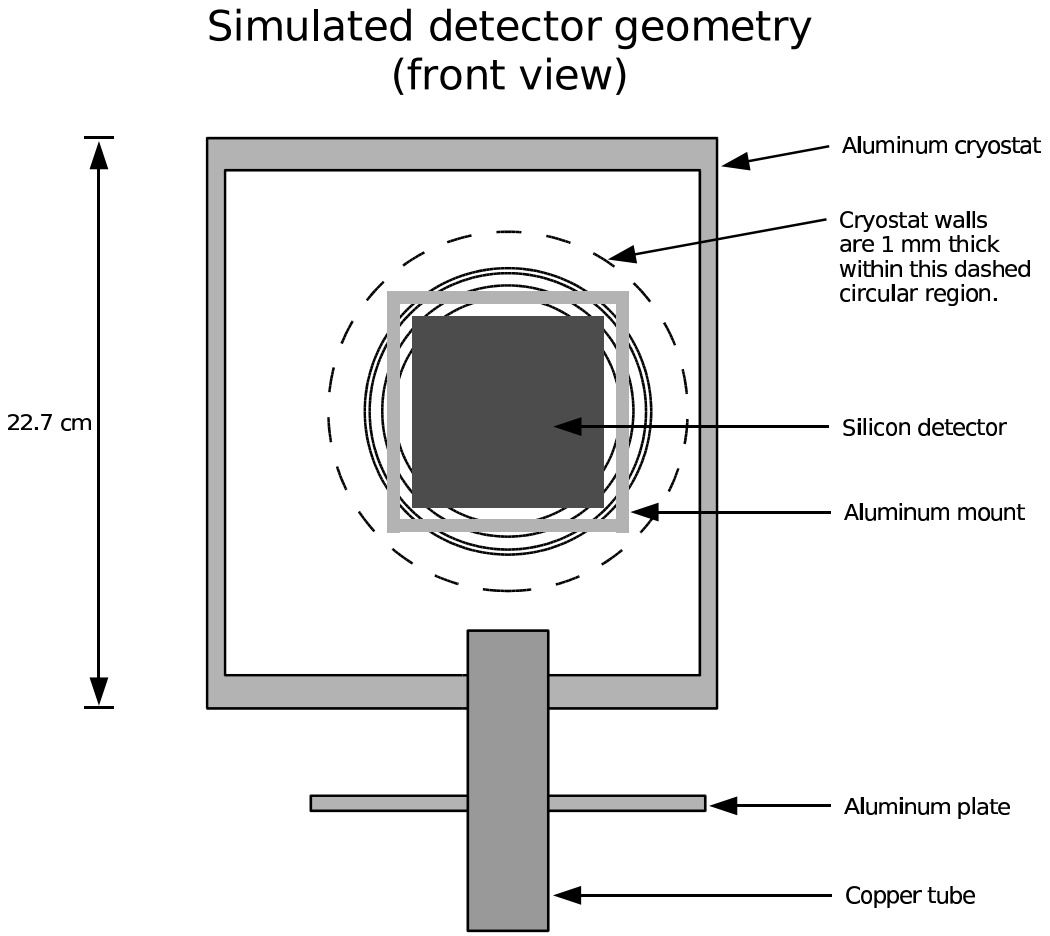

Figure 2: Simulated detector geometry for the CCI2 detector, shown as a cross-sectional front view. The cross-section passes through the center point of the front silicon detector crystal. Also indicated on the diagram are the positions of each germanium detector crystal and the position of the aluminum mount for the germanium detector crystals. Each front and back cryostat wall is 1 mm thick within the dashed circular region.

2 Intrinsic photopeak efficiency

The intrinsic photopeak efficiency at a specific energy E is the number of detected events within an energy window of $E \pm 10$ keV, divided by the total number of events with initial energies that are equal to E which are incident upon the active portion of the front silicon detector crystal. Figure 3 shows the simulated result for the intrinsic photopeak efficiency versus energy for the CCI2 detector.

The source photons with initial energy E that interact inside the detector crystals but do not deposit full energy within an energy window of $E \pm 10$ keV partially deposit their energy by Compton scattering and scatter out of the detector crystals. These source photons create a Compton background in the detected energy spectrum at energies below the $E \pm 10$ keV photopeak. Figure 4 shows a simulated energy spectrum for the CCI2 detector for a 662 keV point source which shows the detected 662 ± 10 keV photopeak and the Compton background.

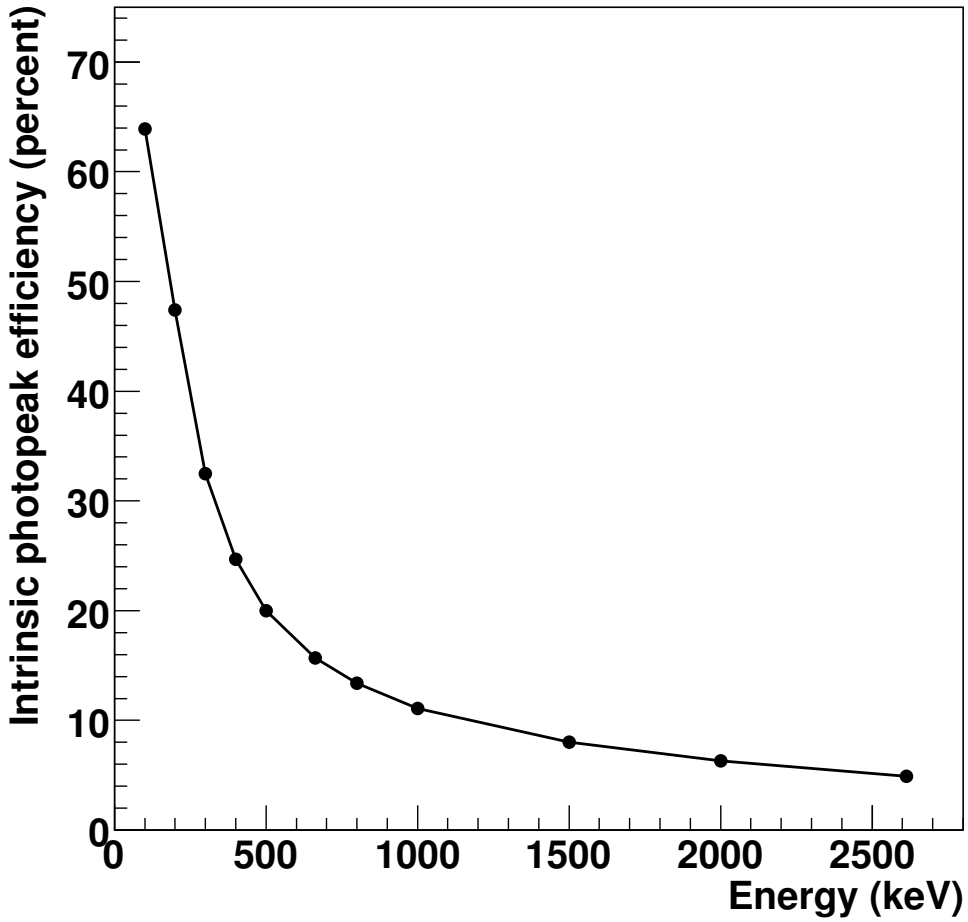

Figure 3: Simulated result for the intrinsic photopeak efficiency versus energy for the CCI2 detector.

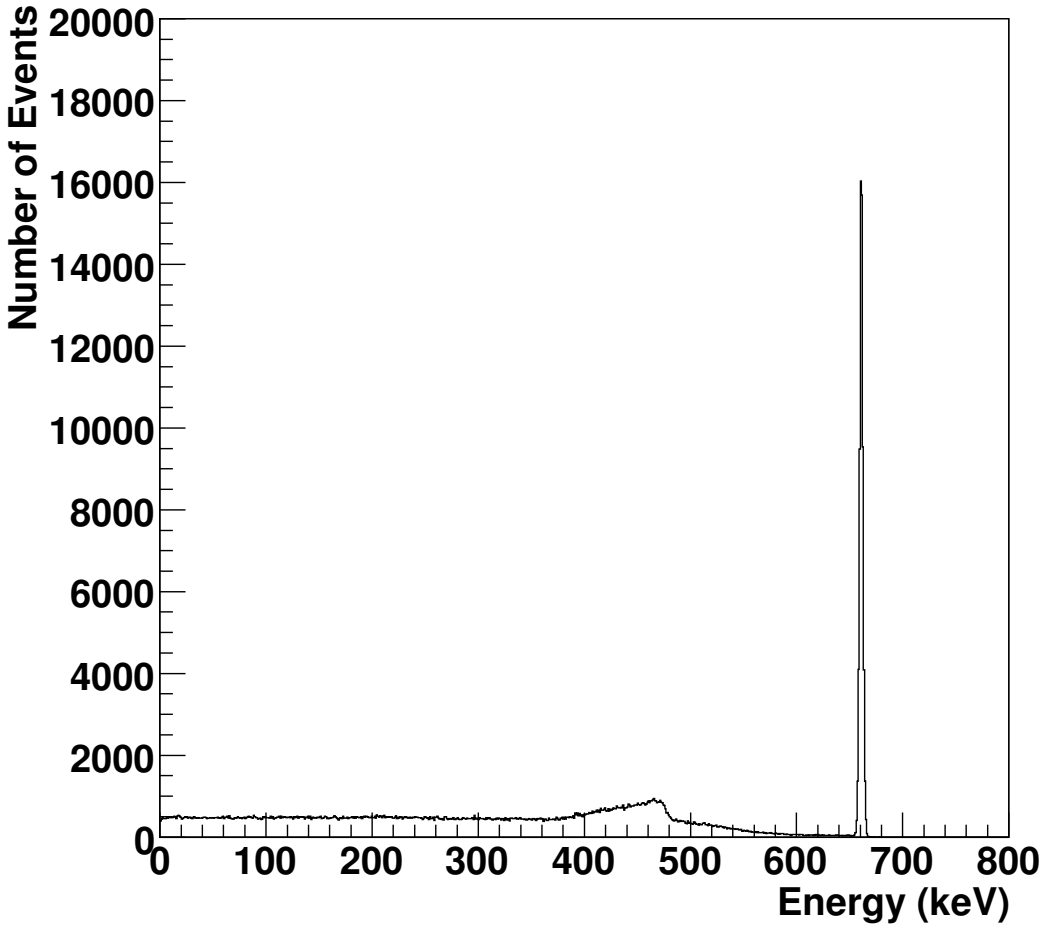

Figure 4: Simulated energy spectrum for the CCI2 detector for a 662 keV point source located 1 meter away from the detector, on the center axis of the detector. The source photons that interact inside the detector crystals but do not deposit full energy within an energy window of 662$\pm$10 keV partially deposit their energy by Compton scattering and scatter out of the detector crystals. These source photons create a Compton background in the detected energy spectrum at energies below the 662$\pm$10 keV photopeak.

3 Imaging efficiency

The imaging efficiency at a specific energy E is defined as the number of detected events within the signal region, divided by the total number of signal events that have initial energies equal to E which are incident upon the active portion of the front silicon detector crystal. The signal region size is defined using the angular distance of closest approach (DOCA) of an image ring to the exact source location. The Compton scattering angle of the first interaction and the positions of the first two interactions of an event define the opening angle and axis direction of a cone. This cone is back-projected onto a sphere which is centered at the detector. The intersection of the cone and the sphere is a Compton image ring, which is a ring-shaped curve that is nearly circular if the radius of the sphere is large compared to the detector length scale. The signal region size is defined by specifying the signal region radius as the angular distance away from the exact source location such that 85% of the total number of signal image rings have DOCA angles within the signal region radius. Table 1 shows simulated results for the signal region radius for the CCI2 detector for various energies. Improving the energy resolution and the position resolution of interactions within the detector crystals reduces the size of the signal region, because decreasing the uncertainties in interaction energies and positions decreases the amount by which an image ring is shifted away from the exact source location.

Imaged events must pass the following event selection requirements. The event energy deposited in the detector crystals must be within a $\pm$10 keV energy-cut window centered at the initial source photon energy. An event must produce at least two interactions in the detector crystals to be imaged. The first two interactions give the directional information of the incident photon. The total energy deposition for an event is the sum of all energy deposits for all interactions within the detector crystals. If the first two interactions for an event occur within the same pixel, then that event is rejected. If the first two interactions for an event are both within the same detector crystal, then the two interactions must be separated by at least 4 pixel widths. Figure 5 shows the simulated result for the imaging efficiency versus energy for the CCI2 detector.

Energy (keV)	Signal region radius (degrees)
100	14.5
200	10.75
300	8.75
400	8.0
500	7.0
662	6.5
800	6.25
1000	6.0
1500	5.5
2000	5.25
2614	5.0

Table 1: Simulated results for the signal region radius for the CCI2 detector for various energies. For each energy, the source is a point source located 1 meter away from the detector, on the center axis of the detector.

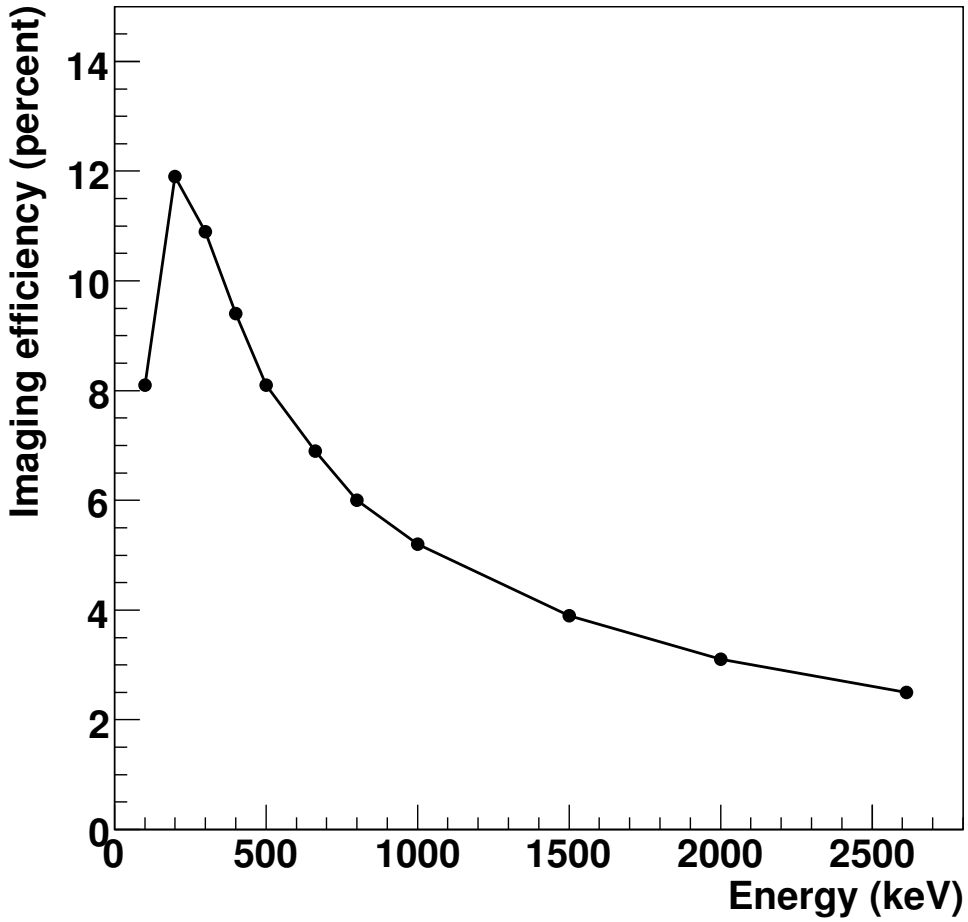

Figure 5: Simulated result for the imaging efficiency versus energy for the CCI2 detector, for a point source located 1 meter away from the detector, on the center axis of the detector.

4 Angular Resolution Metric (ARM)

The ARM angle for an event is defined as ARM = $\alpha_C - \alpha_g$ where α_C is the Compton scattering angle of the first interaction which is determined by the Compton scattering equation using detected interaction energies, and α_g is the geometrical scattering angle of the first interaction which is determined using the source location and the detected positions of the first two interactions.

Figure 6 shows a simulated ARM distribution for the CCI2 detector for 662 keV image events using a 662 keV point source with a source angle of 0 degrees, and the FWHM of the ARM distribution is 3.6 degrees. The source angle is defined as the angle between the source and the axis perpendicular to the front of the detector, in the *xz*-plane. The *xz*-plane is the horizontal plane that passes through the center point of each detector crystal. For all CCI2 simulations, the source is always located in the *xz*-plane, and the separation distance between the source and the front of the detector is always 1 meter. A source angle of 0 degrees corresponds to the source located directly on the center axis of the detector. Table 2 shows FWHM results for simulated ARM distributions for the CCI2 detector for image events, for five different energies, for various source angles for each energy.

Improving the energy resolution and the position resolution of interactions within the detector crystals reduces the FWHM of an ARM distribution, because decreasing the uncertainties in interaction energies and positions decreases the amount by which α_C and α_g are shifted away from their exact values.

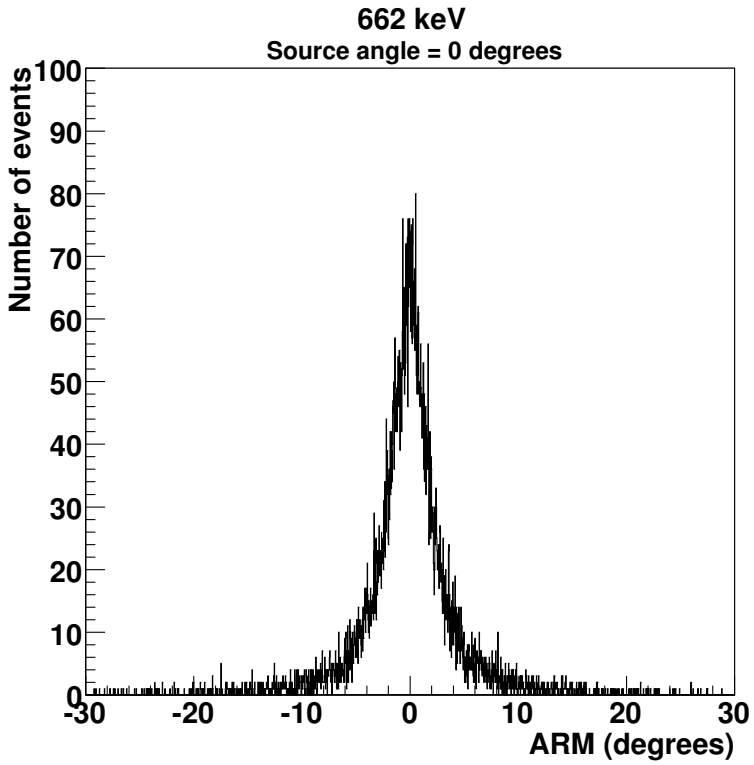

Figure 6: Simulated ARM distribution for the CCI2 detector for 662 keV image events using a 662 keV point source with a source angle of 0 degrees, and the FWHM of the ARM distribution is 3.6 degrees.

Energy (keV)	Source angle (degrees)	FWHM of ARM distribution (degrees)
186	0	7.2
	15	7.1
	30	7.2
	45	8.1
	60	8.3
	75	8.7
414	0	4.2
	15	4.2
	30	4.6
	45	5.5
	60	5.8
	75	6.1
662	0	3.6
	15	3.5
	30	3.6
	45	4.0
	60	4.2
	75	4.8
1000	0	3.2
	15	3.2
	30	3.4
	45	4.2
	60	4.4
	75	4.6
2614	0	2.9
	15	2.9
	30	3.0
	45	3.2
	60	3.3
	75	3.9

Table 2: FWHM results for simulated ARM distributions for the CCI2 detector for image events, for five different energies, for various source angles for each energy. The source angle is defined as the angle between the source and the axis perpendicular to the front of the detector, in the *xz*-plane. The *xz*-plane is the horizontal plane that passes through the center point of each detector crystal. For each result, the source is located in the *xz*-plane, and the separation distance between the source and the front of the detector is 1 meter. A source angle of 0 degrees corresponds to the source located directly on the center axis of the detector.

5 Images

Simulated images are created by plotting the detected image rings from a point source for the entire 4π steradians field of view of the detector. The Compton scattering angle of the first interaction and the positions of the first two interactions of an event define the opening angle and axis direction of a cone. This cone is back-projected onto a sphere which is centered at the detector. The intersection of the cone and the sphere is a Compton image ring, which is a ring-shaped curve that is nearly circular if the radius of the sphere is large compared to the detector length scale.

Figures 7 - 16 show simulated images for the CCI2 detector for point sources with energies of 186, 414, 662, 1000, and 2614 keV, for source angles of 0, 15, 30, 45, 60, and 75 degrees for each energy. Each image shows the entire 4π steradians field of view of the detector projected onto a planar 2-dimensional plot, with angles along each axis represented using the coordinates θ and ϕ. The angle θ is the altitude angle above or below the horizontal *xz*-plane, and ϕ is the azimuth angle within the *xz*-plane. On each image, the source angle is represented by the angle ϕ. The source angle is defined as the angle between the source and the axis perpendicular to the front of the detector, in the *xz*-plane. The *xz*-plane is the horizontal plane that passes through the center point of each detector crystal. For all CCI2 simulations, the source is always located in the *xz*-plane, and the separation distance between the source and the front of the detector is always 1 meter. A source angle of 0 degrees corresponds to the source located directly on the center axis of the detector. Each image is a plot of all of the image rings of a point source, and a large number of image rings are plotted on each image so that image rings fill the entire plot. The color scale on each image shows the number of overlapping image rings per image pixel on the plot. The largest number of overlapping rings per pixel occurs near the source position. Uncertainties in the detected interaction energies and interaction positions within the detector crystals cause the image rings to be shifted away from the exact source position, so many of the image rings in an image do not overlap the exact source position. Thus, the image of a point source is distributed over an angular region surrounding the exact source position.

The image angular resolution of the detector is found to improve as the source energy increases. For each energy, the image angular resolution is found to become progressively worse as the source angle is increased beyond 15 degrees.

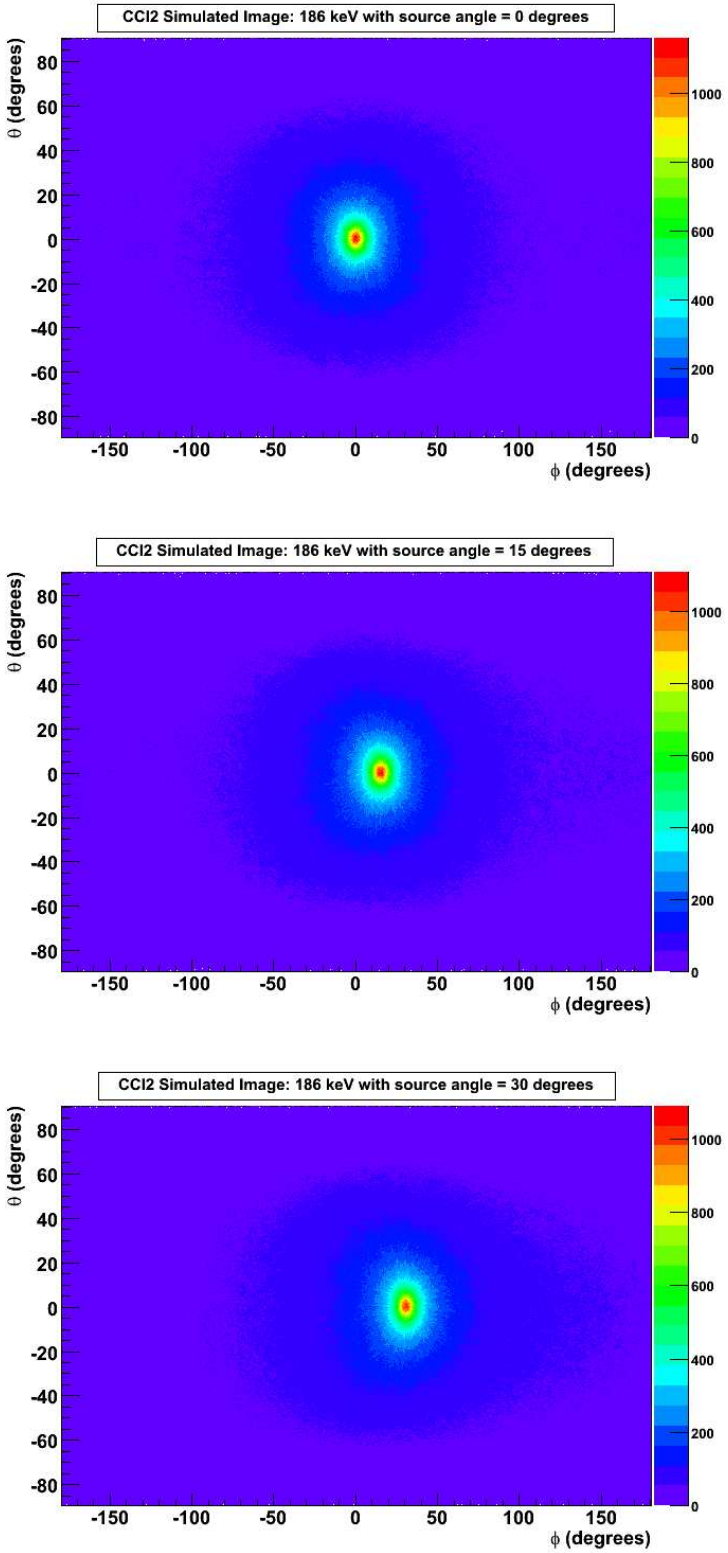

Figure 7: Simulated images for the CCI2 detector, each showing a 186 keV point source, and the individual images are for source angles of 0 degrees (top), 15 degrees (middle), and 30 degrees (bottom).

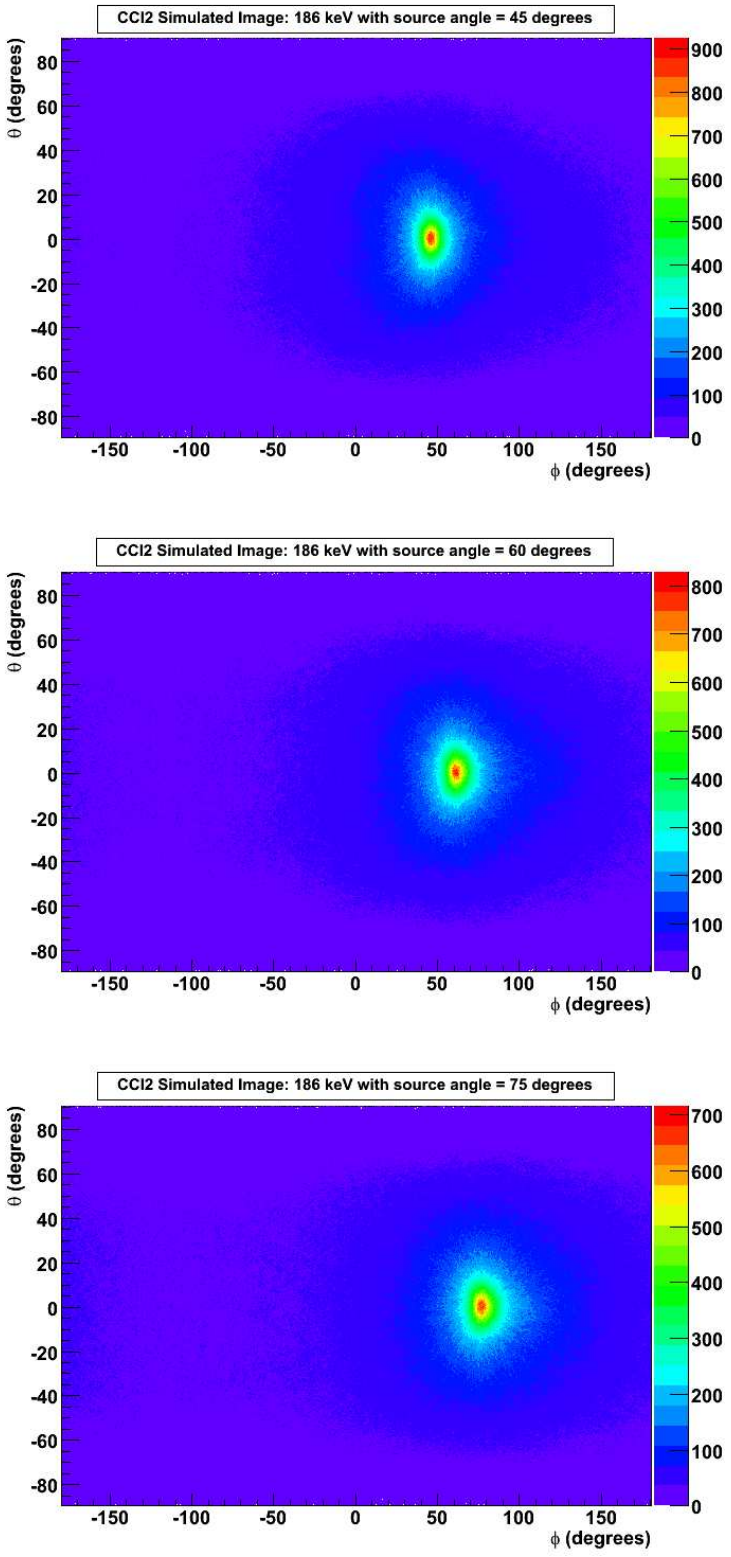

Figure 8: Simulated images for the CCI2 detector, each showing a 186 keV point source, and the individual images are for source angles of 45 degrees (top), 60 degrees (middle), and 75 degrees (bottom).

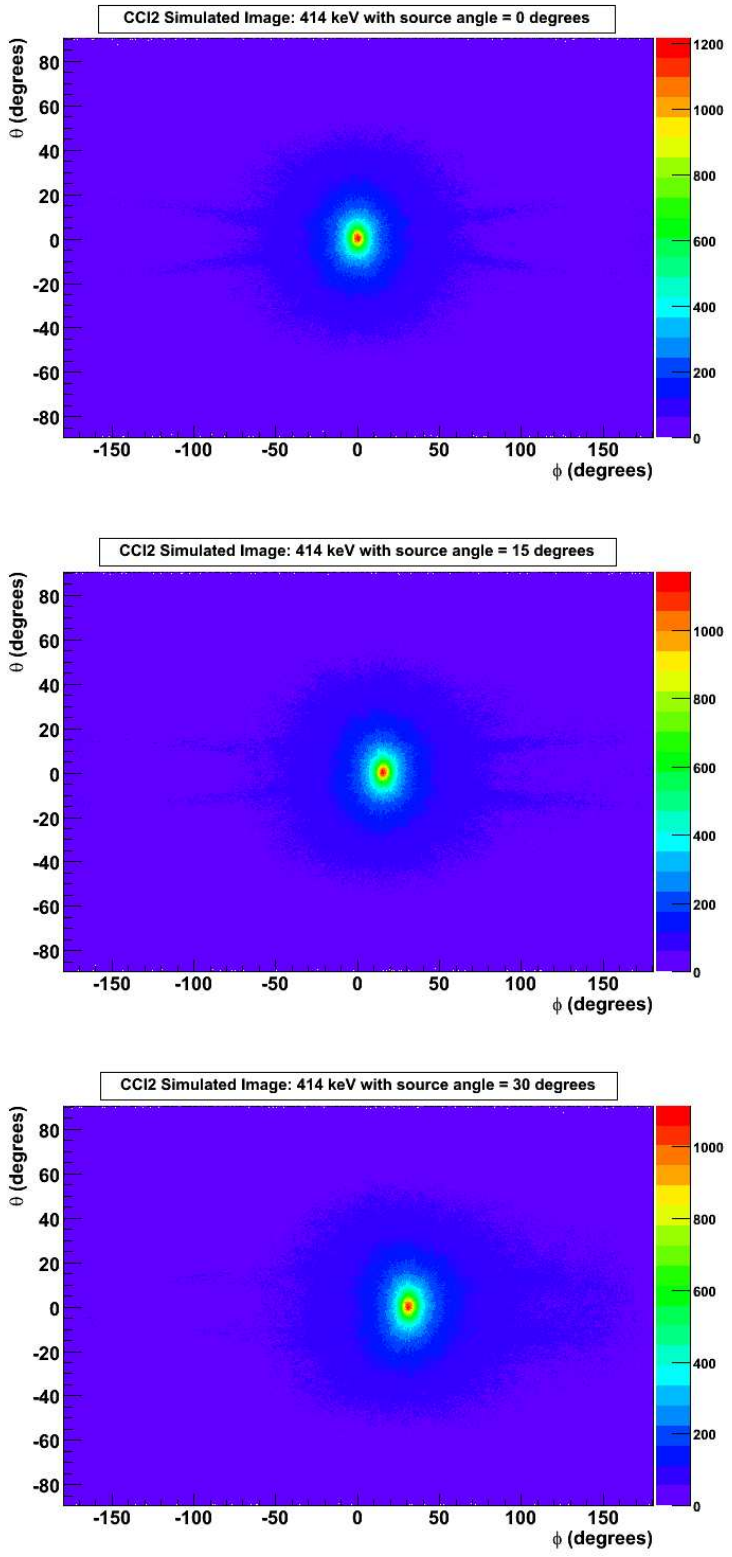

Figure 9: Simulated images for the CCI2 detector, each showing a 414 keV point source, and the individual images are for source angles of 0 degrees (top), 15 degrees (middle), and 30 degrees (bottom).

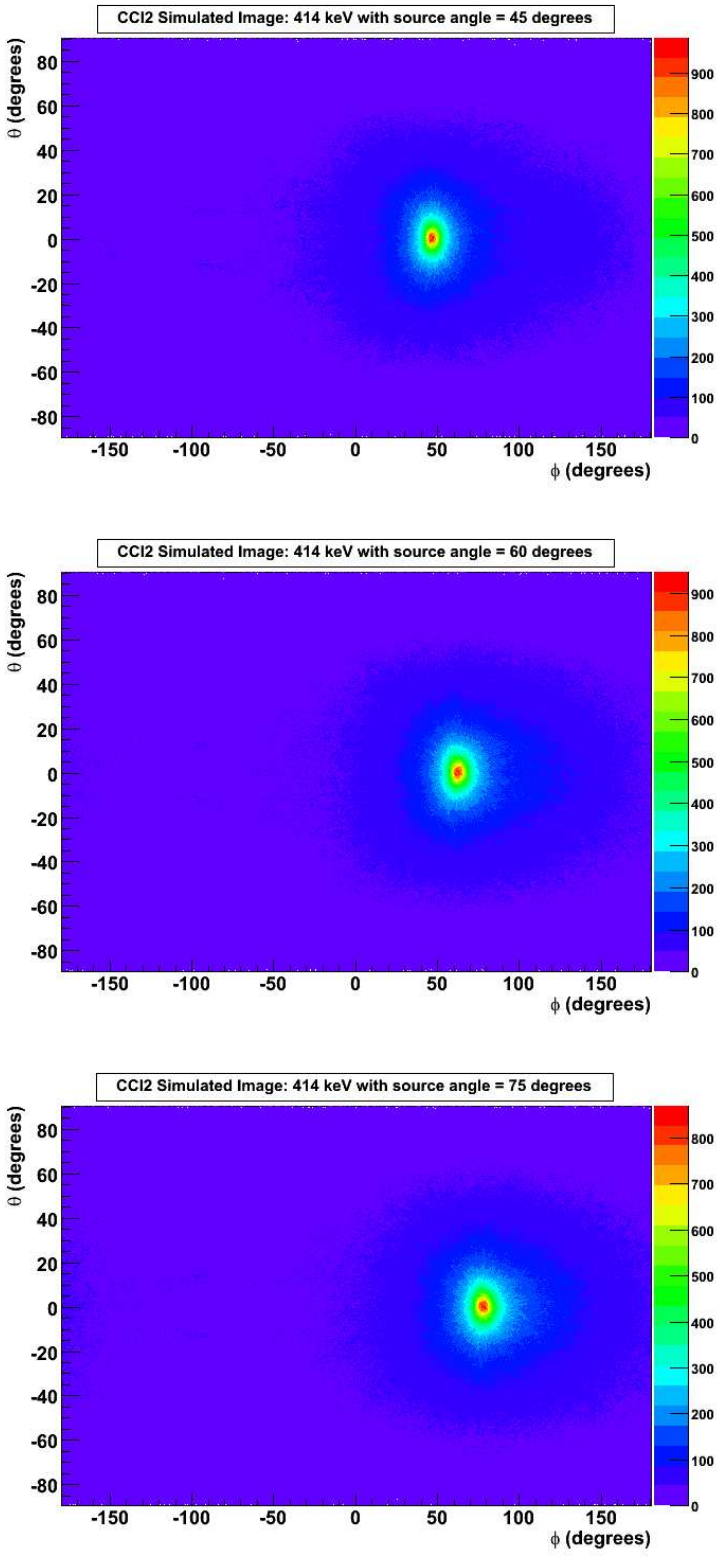

Figure 10: Simulated images for the CCI2 detector, each showing a 414 keV point source, and the individual images are for source angles of 45 degrees (top), 60 degrees (middle), and 75 degrees (bottom).

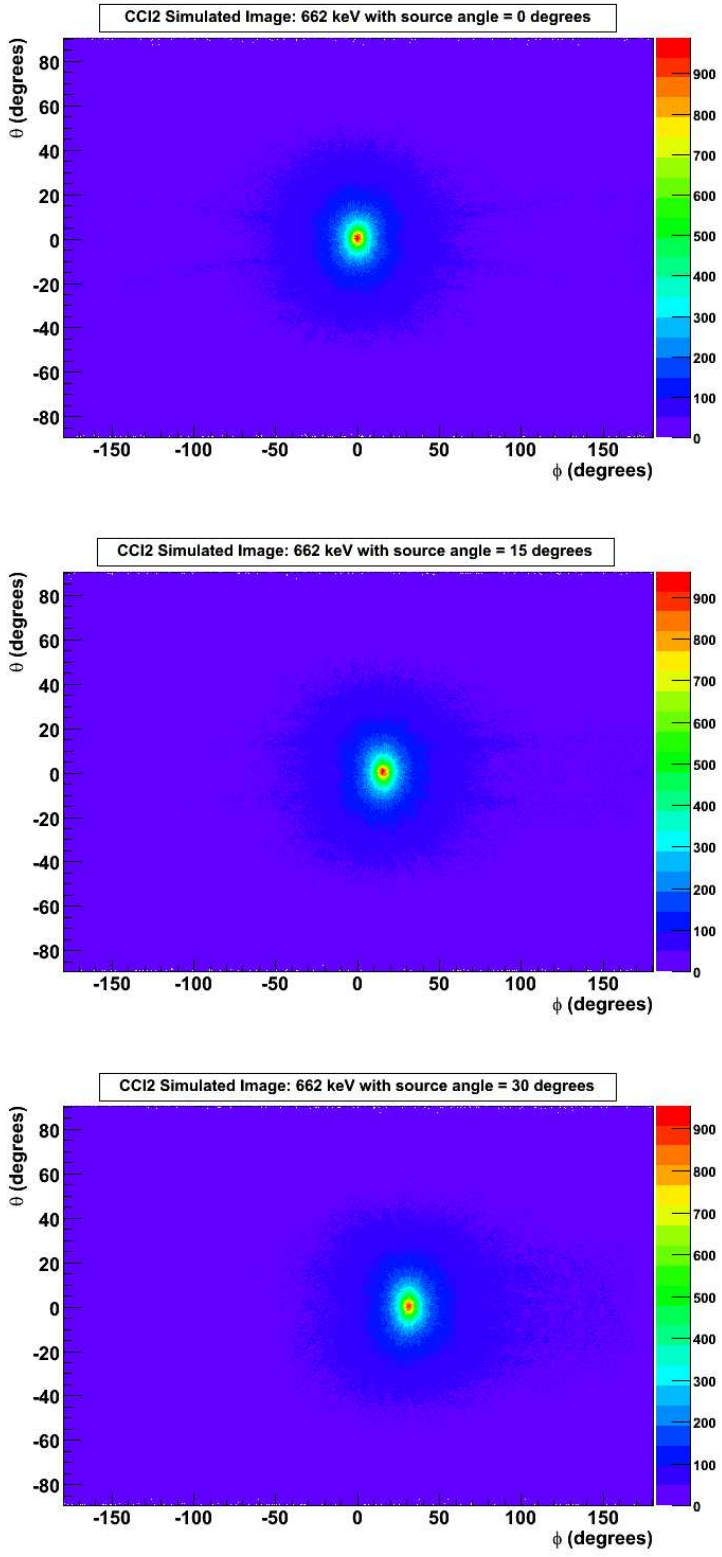

Figure 11: Simulated images for the CCI2 detector, each showing a 662 keV point source, and the individual images are for source angles of 0 degrees (top), 15 degrees (middle), and 30 degrees (bottom).

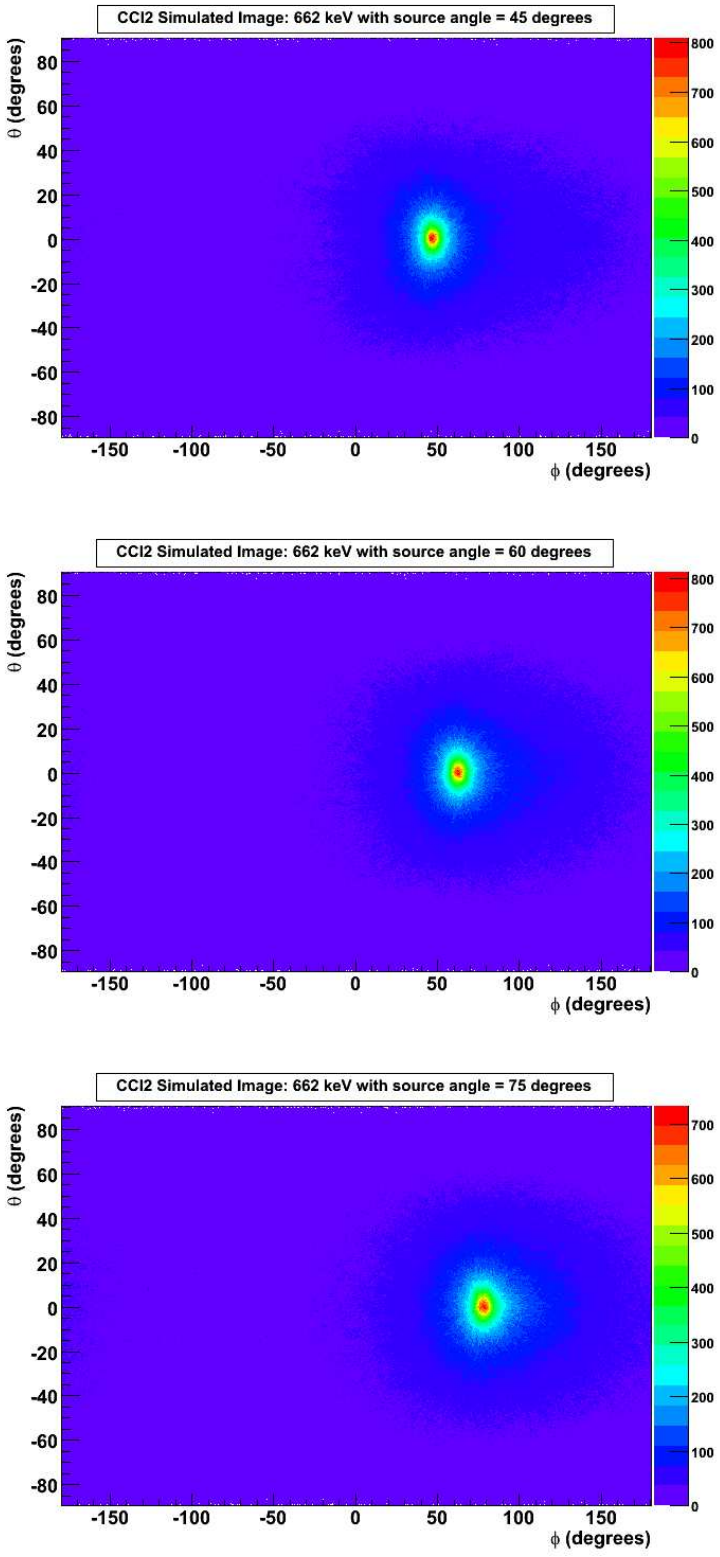

Figure 12: Simulated images for the CCI2 detector, each showing a 662 keV point source, and the individual images are for source angles of 45 degrees (top), 60 degrees (middle), and 75 degrees (bottom).

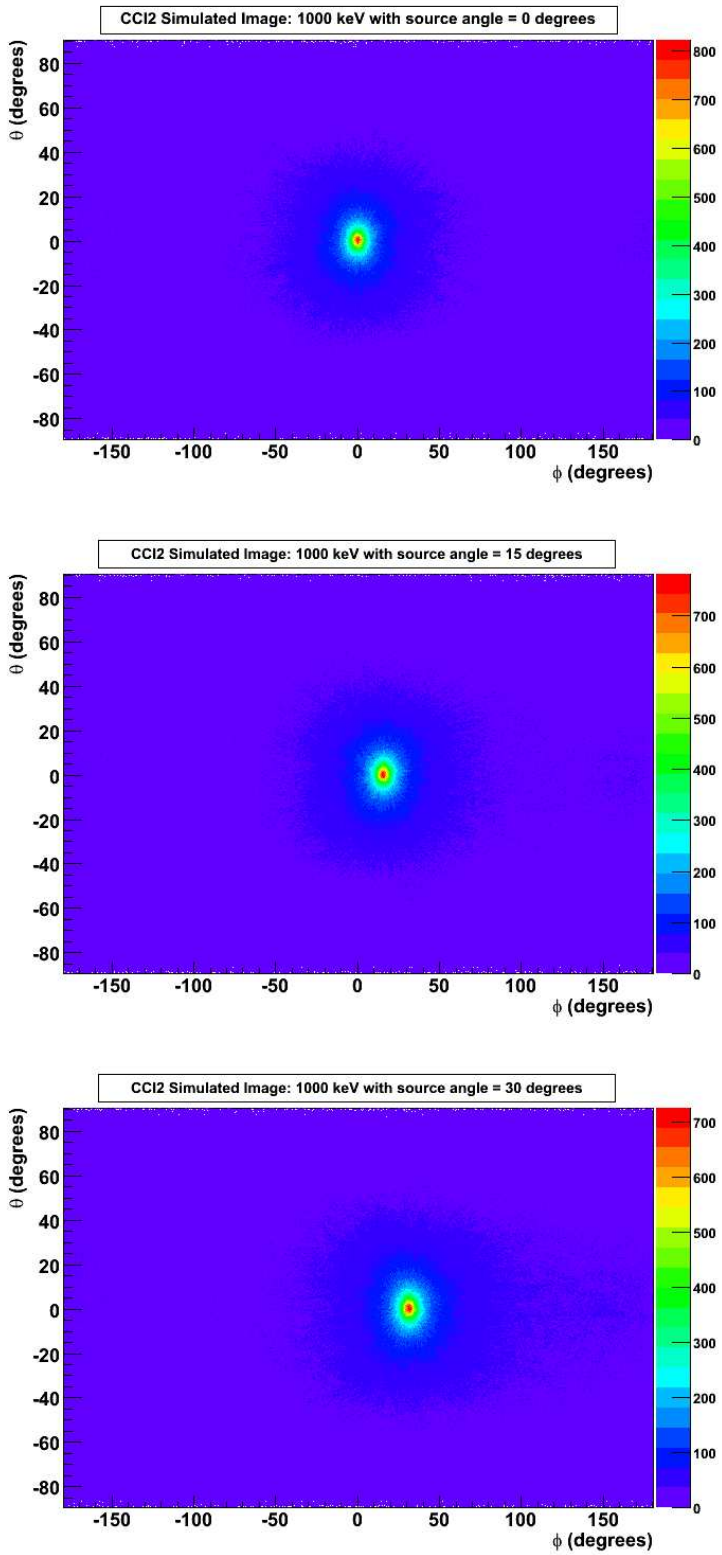

Figure 13: Simulated images for the CCI2 detector, each showing a 1000 keV point source, and the individual images are for source angles of 0 degrees (top), 15 degrees (middle), and 30 degrees (bottom).

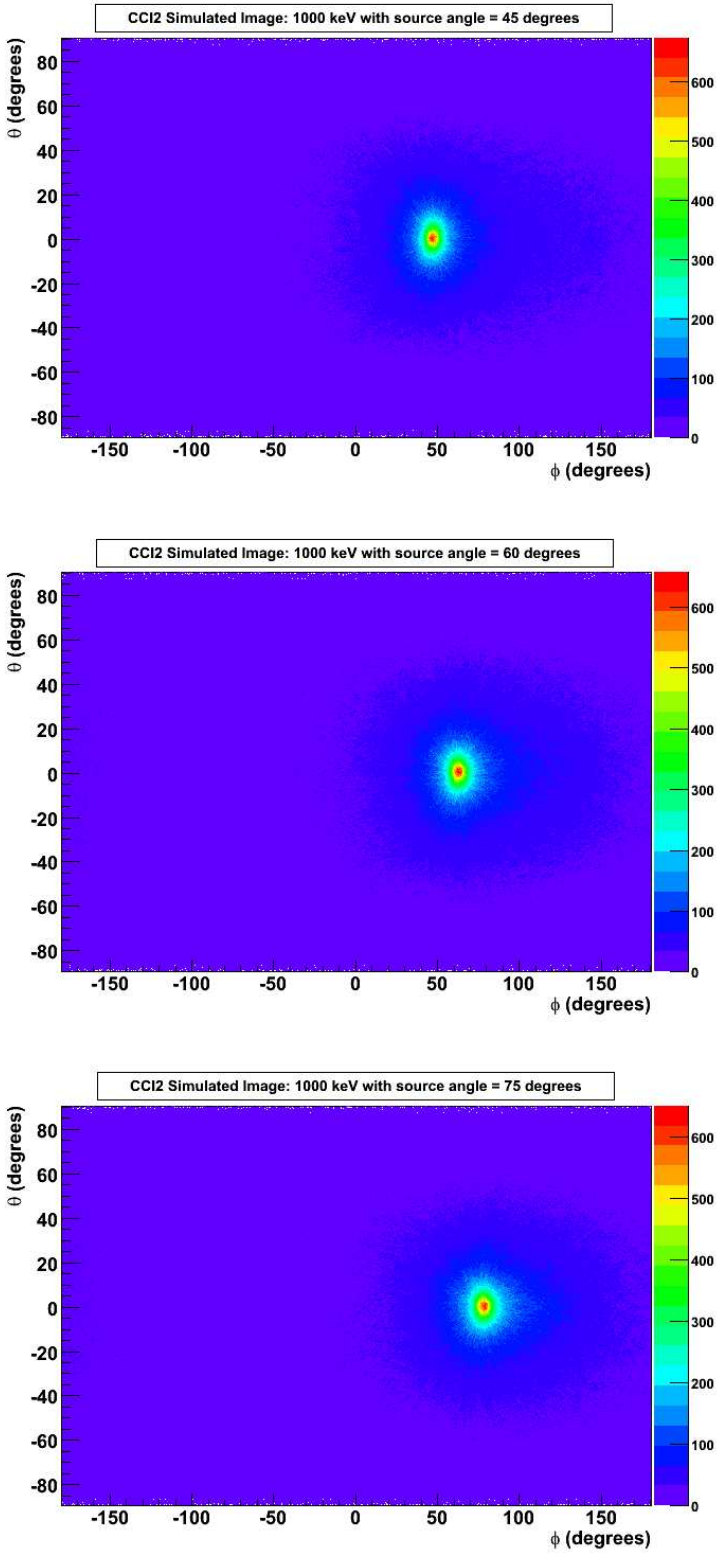

Figure 14: Simulated images for the CCI2 detector, each showing a 1000 keV point source, and the individual images are for source angles of 45 degrees (top), 60 degrees (middle), and 75 degrees (bottom).

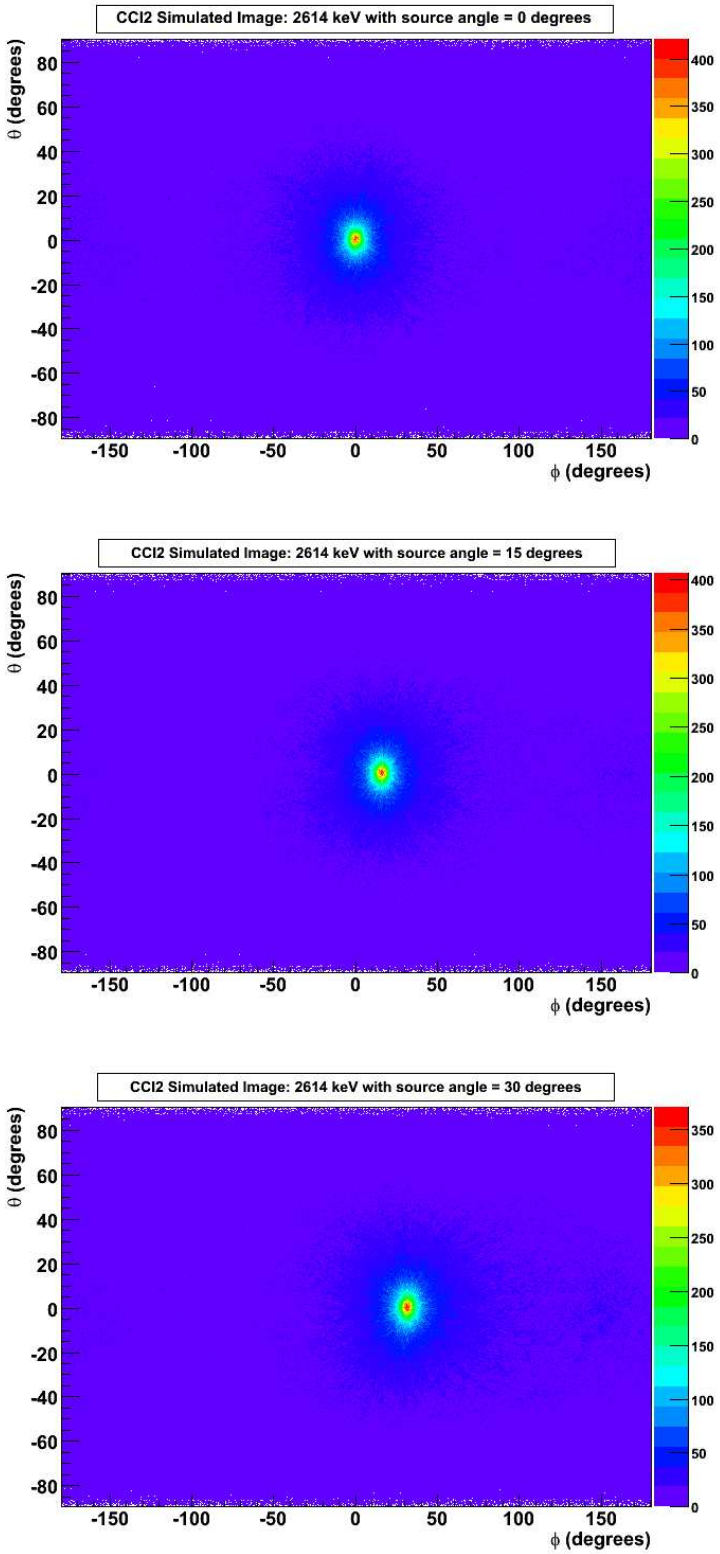

Figure 15: Simulated images for the CCI2 detector, each showing a 2614 keV point source, and the individual images are for source angles of 0 degrees (top), 15 degrees (middle), and 30 degrees (bottom).

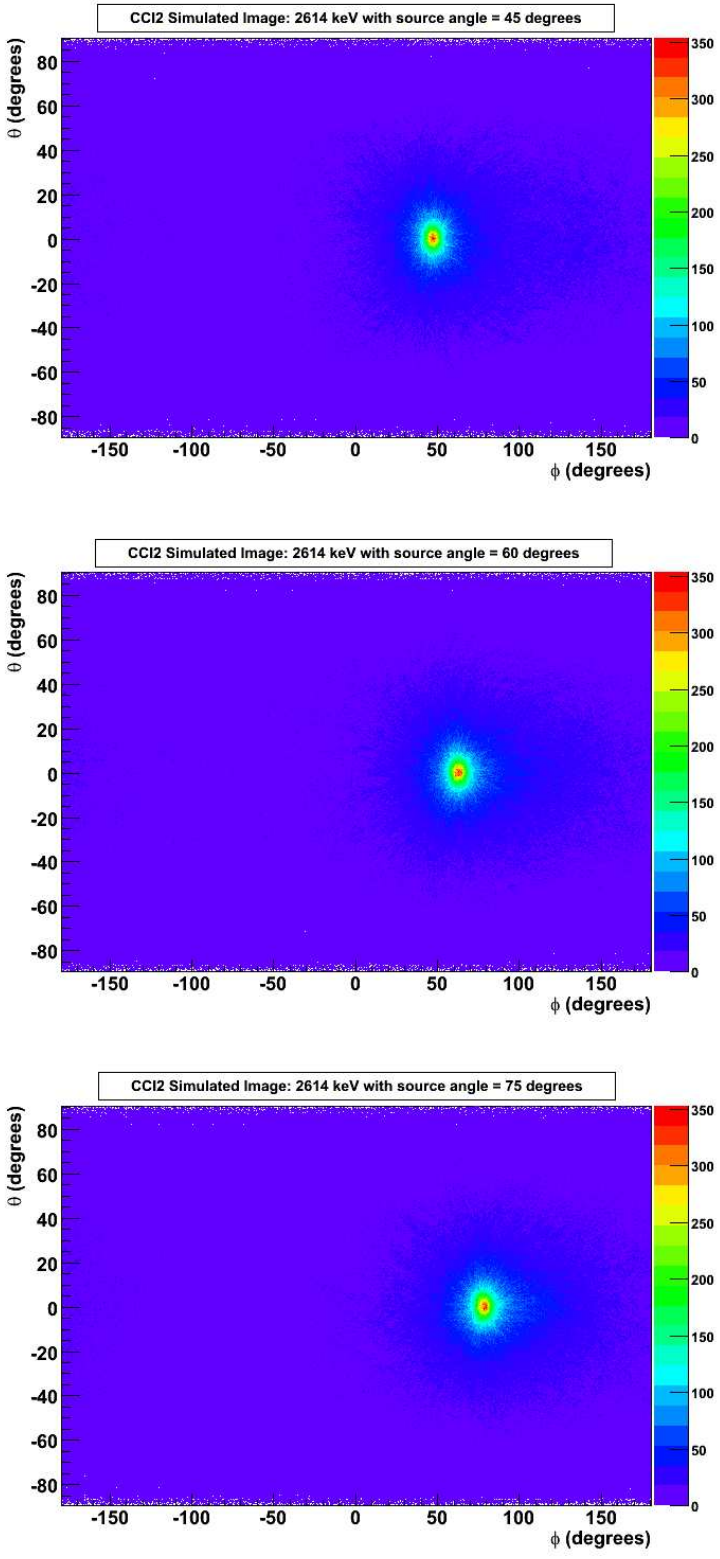

Figure 16: Simulated images for the CCI2 detector, each showing a 2614 keV point source, and the individual images are for source angles of 45 degrees (top), 60 degrees (middle), and 75 degrees (bottom).